

1 Tropical Pacific warming patterns influence future hydroclimate shifts and  
2 extremes in the Americas

3  
4  
5 Ulla K. Heede<sup>1\*</sup>, Nathan Lenssen<sup>2,3,4</sup>, Kristopher B. Karnauskas<sup>1,2</sup> and Clara Deser<sup>4</sup>

6  
7 <sup>1</sup> Cooperative Institute for Research in Environmental Sciences, University of Colorado,  
8 Boulder, CO, USA

9 <sup>2</sup> Department of Atmospheric and Oceanic Sciences, University of Colorado, Boulder, CO, USA

10 <sup>3</sup> Department of Applied Mathematics and Statistics, Colorado School of Mines, Golden, CO,  
11 USA

12 <sup>4</sup> National Center for Atmospheric Research, Boulder, CO, USA  
13  
14  
15

16 **Abstract**

17  
18 The eastern tropical Pacific (ETP) Ocean is projected to warm faster than the Atlantic or Indian  
19 Oceans in the 21<sup>st</sup> century, yet this prediction is highly uncertain due to model-observation  
20 discrepancies. The potential impacts of this uncertainty on regional terrestrial hydroclimates are  
21 largely unknown, which is problematic for climate risk assessments. To address this, we  
22 designed novel atmospheric model experiments simulating future global warming with and  
23 without enhanced ETP warming, superimposed upon an idealized El Niño-Southern Oscillation  
24 (ENSO) cycle. Our results show that enhanced ETP warming significantly influences future  
25 terrestrial hydroclimates in several regions across the Americas. In southern Mexico, Central  
26 America and the Amazon region, enhanced ETP warming exacerbates long term drought trends  
27 and extreme drought events, while the opposite is true in south-central South America. Along the  
28 west coast of the continental United States, the effects of enhanced ETP warming manifest as El  
29 Niño-related extreme precipitation anomalies. These findings illustrate how climate impact  
30 projections may be misrepresented in conventional multi-model analysis, which does reflect true  
31 uncertainty of the future tropical Pacific warming pattern.  
32  
33  
34

35 \* Corresponding Author: Ulla K. Heede, 4001 Discovery Dr, Boulder, Colorado,  
36 ulla.heede@colorado.edu  
37  
38  
39

40  
41  
42  
43  
44  
45  
46  
47  
48  
49  
50  
51  
52  
53  
54  
55  
56  
57  
58  
59  
60  
61  
62  
63  
64  
65  
66  
67  
68  
69  
70  
71  
72  
73  
74  
75  
76  
77  
78

### **Plain Language Summary**

How the tropical Pacific responds to global warming is uncertain because models and observations do not agree. Models predict an enhanced warming of the eastern tropical Pacific, yet observations show the opposite trend. This uncertainty may propagate into uncertainty in regional precipitation patterns, which have consequences for society's ability to adapt to climate change. We designed two model experiments with (EP) and without (noEP) enhanced eastern tropical Pacific warming to understand how ocean warming patterns affect precipitation in the Americas. We found that droughts were intensified in Central America and the Amazon region in the EP experiment compared to the noEP experiment (i.e., when the tropical Pacific warms up faster, droughts intensify in those regions), yet reduced in south-central South America. Next, we looked at changes to extreme events, and found that during El Nino years, drought extremes were exacerbated more in the EP relative to the noEP experiment in the Amazon, while wet extremes were exacerbated along the continental U.S. West Coast. These results show how the uncertainty in future ocean warming patterns can propagate into uncertainty for terrestrial precipitation trends and changes to extremes. This finding has consequences for society's ability to adapt to future climate change.

### **Key Points:**

1. Here we show how uncertainty in the future tropical Pacific warming pattern propagates into future changes to terrestrial hydro-climates.
2. Enhanced eastern Pacific warming, as simulated by models, exacerbates droughts in Central America and the Amazon region.
3. Extreme precipitation events occurring in several regions during El Nino years are modulated by the background Pacific warming pattern.

79  
80  
81

## 82 **Introduction**

83

84 Precipitation variability is one of the most societally impactful aspects of contemporary climate,  
85 yet it remains one of the most difficult to predict. Persistent droughts can alter regional biomes  
86 (Vicente-Serrano *et al.*, 2013), while short term extreme drought or flooding events can create  
87 severe challenges for agriculture (Devereux, 2007; Watanabe *et al.*, 2018), water management  
88 (Crochemore, Ramos and Pappenberger, 2016), human health (Harp *et al.*, 2021; Buchwald *et*  
89 *al.*, 2022), natural hazard safety (Nadim *et al.*, 2006; Hong *et al.*, 2007) and economic production  
90 (Kotz *et al.*, 2022). Despite the importance of understanding precipitation changes for successful  
91 adaption to climate change, projecting the response of precipitation to anthropogenic radiative  
92 forcing is among our greatest scientific challenges.

93

94 Some aspects of the hydrological response to global warming are robust, such as the global  
95 increase in water vapor following the Clausius-Clapeyron relation, which in turn is shown to  
96 increase precipitation and evaporation rates by 2% per degree warming on average (Held and  
97 Soden, 2006). However, this scaling estimate is global and does not specify where precipitation  
98 increases take place. Assuming a static background state of moisture transport and convergence,  
99 a framework of ‘wet gets wetter’ has been proposed, in which areas of global moisture  
100 convergence and net positive precipitation minus evaporation (P-E) such as the tropics receive  
101 more precipitation, whereas areas of moisture divergence and negative P-E experience increased  
102 drought (Manabe and Wetherald, 1975; Allen and Ingram, 2002; Wetherald and Manabe, 2002;  
103 Chou and Neelin, 2004; Held and Soden, 2006).

104  
105 However, several studies have shown that observed precipitation trends are not consistent with  
106 the wet-gets-wetter framework, particularly over land (Xie *et al.*, 2010; Greve *et al.*, 2014; Pfahl,  
107 O’Gorman and Fischer, 2017). The wet-gets-wetter argument is a result of assuming spatially  
108 homogeneous changes in surface temperature, neglecting the spatially varying warming of the  
109 Earth’s surface under external forcing and the circulation changes that such temperature  
110 gradients induce, which may greatly impact the regional precipitation response.

111  
112 In general, land warms faster than the sea surface, polar regions warm faster than the subtropics,  
113 and the Northern Hemisphere has warmed more than the Southern Hemisphere over the  
114 industrial era (Lenssen *et al.*, 2019; Gulev *et al.*, 2021; Morice *et al.*, 2021). In addition, the  
115 ocean has experienced heterogeneous warming rates throughout the observational record as the  
116 subpolar North Atlantic, the east/central equatorial Pacific and the Southern Ocean show flat or  
117 cooling trends in recent decades (Dong and Lu, 2013; Keil *et al.*, 2020; Dong *et al.*, 2022) while  
118 the Indian Ocean has experienced accelerated warming since 1950 (Hu and Fedorov, 2019;  
119 Zhang *et al.*, 2019). These unequal warming rates cause anomalous surface temperature  
120 gradients which in turn alter the large-scale atmospheric circulation and ultimately the transport  
121 and convergence of moisture and subsequent precipitation.

122  
123 The future pattern of sea surface temperature (SST) changes in the tropical Pacific is of  
124 particular concern as this region contains the largest convective zone on the planet and has been  
125 widely recognized as a key driver of global weather and climate variability as early as Walker  
126 (Walker, 1925). More recently, using the Green’s function, the radiative response to surface  
127 warming in the western tropical Pacific has been identified as a key driver of global climate

128 sensitivity (Dong *et al.*, 2019; Bloch-Johnson *et al.*, 2024). Yet, how the tropical Pacific will  
129 respond to anthropogenic radiative forcing is uncertain (DiNezio, Clement and Vecchi, 2010;  
130 Seager *et al.*, 2019; Heede and Fedorov, 2021; Wills *et al.*, 2022). Over the satellite era, the  
131 eastern tropical Pacific has experienced a lack of warming, while adjacent ocean regions have  
132 warmed, resulting in accelerated trade winds along the equatorial Pacific (Dong and Lu, 2013;  
133 Kosaka and Xie, 2013; Heede and Fedorov, 2023a). This multi-decadal trend is thought to be a  
134 combination of natural variability, a transient response to greenhouse gas forcing (typically  
135 dubbed the ‘ocean dynamical thermostat’ mechanism: Clement *et al.* 1996; Sun and Liu 1996;  
136 Heede *et al.* 2020; Heede and Fedorov 2023a), anthropogenic aerosols (Hwang *et al.*, 2024;  
137 Watanabe *et al.*, 2024) and Southern Ocean cooling (Dong *et al.*, 2022; Kang *et al.*, 2023).  
138 However, such a trend pattern is rarely captured by historical simulations produced by global  
139 coupled climate models (Seager *et al.*, 2022; Wills *et al.*, 2022). On the contrary, models predict  
140 an enhanced eastern Pacific warming, emerging in the 21st century (Heede and Fedorov, 2021;  
141 Wu *et al.*, 2021; Ying *et al.*, 2022), and this is argued to be caused by a slowdown of tropical  
142 circulation (Vecchi and Soden, 2007) and a slowdown in the oceanic subtropical cells (Heede,  
143 Fedorov and Burls, 2020). Whether and when the observed trend will reverse and an enhanced  
144 eastern Pacific warming emerge is, however, uncertain, given the inability of the same models to  
145 capture the observed trends. Overall, this uncertainty hinders robust projections of global  
146 dynamical changes driven by tropical Pacific warming trends, and limits our ability to  
147 understand the full potential spectrum of future rainfall projections with consequences for  
148 societal adaptation.

149

150 While the sensitivity of precipitation trends in the Americas to Pacific warming patterns has been  
151 investigated in general (Seager and Vecchi, 2010), the consequences of the current model-  
152 observational discrepancy have not been quantitatively investigated from a climate impacts  
153 focused perspective. While studies have considered large-scale climatic and precipitation  
154 responses to various ocean warming patterns in the tropical Pacific (Zhang *et al.*, 2019; Fosu, He  
155 and Liguori, 2020), much less attention has been paid to the terrestrial and regional precipitation  
156 responses, which is more important for assessing climate impacts. The agreement on enhanced  
157 eastern Pacific warming in CMIP6 models means that the spread among models, and the  
158 resulting science using these models, does not capture the true uncertainty associated with the  
159 tropical Pacific warming response with perilous consequences for society's ability to plan for a  
160 wider range of possible future hydroclimatic changes. In this study, we present results from a set  
161 of novel climate model experiments that addresses this issue, and in which the climate impacts  
162 specifically associated with enhanced eastern Pacific warming can be evaluated while keeping  
163 other factors unchanged.

164  
165 An ubiquitous challenge in projecting precipitation is that precipitation is highly variable across  
166 space and time (Meehl, Wheeler and Washington, 1994; Pendergrass *et al.*, 2017; He and Li,  
167 2019; Schwarzwald *et al.*, 2021). For many human and natural systems, including agriculture  
168 and water management, the seasonality and timing of precipitation is just as important as the  
169 total amount. That is, changes in total precipitation can result in very different outcomes if the  
170 increased precipitation is delivered in extreme events or smaller more frequent events (Livneh *et*  
171 *al.*, 2024) and delivered as snow or rain (Lesk, Coffel and Horton, 2020). Thus, to achieve

172 relevant information about precipitation changes in response to global warming, it is necessary to  
173 understand changes in the variability of precipitation in addition to long term averaged trends.

174  
175 One of the largest drivers of global precipitation variability is the El Niño Southern Oscillation  
176 (ENSO), whose atmospheric component modulates the east-west Walker cell and the north-south  
177 Hadley circulation (Bjerknes, 1969; Ropelewski and Halpert, 1987; Mason and Goddard, 2001).  
178 During the positive ENSO phase (El Niño), the Walker circulation slows and shifts eastward.  
179 This moves moisture convergence to the central Pacific, creating droughts in the Maritime  
180 Continent and Australia and increased precipitation in areas of South America (Mason and  
181 Goddard, 2001; Lenssen et al., 2020). Through teleconnections created by changes in  
182 atmospheric planetary waves originating from the tropics, regions beyond the tropics also  
183 experience precipitation anomalies associated with ENSO (Deser *et al.*, 2017; Yeh *et al.*, 2018;  
184 Lenssen *et al.*, 2020).

185  
186 Because ENSO is a coupled phenomenon with multiple oceanic and atmospheric feedback  
187 processes interacting, understanding how ENSO responds to global warming remains  
188 challenging and highly uncertain. While CMIP6 models generally predict a stronger ENSO in  
189 response to global warming (Fredriksen *et al.*, 2020; Cai *et al.*, 2022), large model differences as  
190 well as a comprehensive mechanism for driving these changes is lacking (Heede and Fedorov,  
191 2023b). While the characteristics of ENSO and associated teleconnections itself may change in  
192 response to global warming (e.i. O'Brien and Deser, 2022; Maher *et al.*, 2023), global warming  
193 and changes in the pattern of warming across the tropical Pacific discussed above may also alter  
194 ENSO teleconnections and impacts. For example, more water vapor in the atmosphere is

195 expected to create a more vigorous rainfall response to ENSO events (Yun *et al.*, 2021) as well  
196 as an eastward shift of the El Niño convection because of the higher absolute SST (Zhou *et al.*,  
197 2014). These complex dynamical interactions make it difficult to determine if future changes to  
198 ENSO-related impacts assessed in fully coupled climate model projections are a result of an  
199 enhanced eastern Pacific warming, global warming, or changes to the ENSO amplitude itself  
200 (Bonfils *et al.*, 2015). Given the uncertainty in both the eastern Pacific warming and ENSO  
201 amplitude, it is important to isolate and understand the impacts associated with each.

202  
203 The purpose of this study is to specifically address both the role of enhanced eastern tropical  
204 Pacific warming and its interaction with ENSO in driving future changes in mean and extreme  
205 precipitation over land, thereby bringing the issue of the tropical Pacific into a mitigation and  
206 adaptation relevant context. In the modeling framework (Section 2), we conduct two sets of  
207 atmospheric general circulation model (AGCM) experiments that follow the SSP5-85 emission  
208 scenario from 2015-2100 with (EP) and without (noEP) prescribed enhanced eastern Pacific  
209 warming (Fig 1a, b). In addition, we prescribe an idealized ENSO cycle that is superimposed  
210 upon each of the background warming patterns (Fig 1c,d). We first consider large-scale changes  
211 to hydroclimates across the Americas and the difference between the EP and noEP experiments.  
212 We then illustrate how these changes manifest regionally and seasonally, and finally, we analyze  
213 how the interaction between ENSO and the mean state modulates ENSO related extreme events.  
214 Our goal is to place the ocean warming pattern uncertainty in a climate impacts framework and  
215 hence our results are focused on describing terrestrial hydroclimatic changes observed in  
216 response to the imposed SST patterns. We refer to previous literature for additional analysis and  
217 in-depth theory regarding the underlying dynamical teleconnection mechanisms, which drive

218 tropically-induced changes in atmospheric moisture convergence (Seager and Vecchi, 2010;  
219 Seager, Naik and Vecchi, 2010; Bonfils *et al.*, 2015; Watterson, 2023)

220

221

## 222 **2 Methods**

### 223 *2.1 Experimental design*

224 Our experimental design consists of three A-GCM experiments with prescribed SST, with 5  
225 ensemble members apiece. The three experiments are: a future with global warming and  
226 enhanced eastern Pacific warming (“EP”), a future with global warming but without enhanced  
227 Pacific warming (“noEP”), and a control simulation without time-evolving global warming  
228 (“Control”). SST anomalies associated with an idealized repeating ENSO cycle are  
229 superimposed in each experiment to investigate ENSO impacts as a function of background state  
230 changes. Our experiments are conducted with the atmosphere-land model components of  
231 Community Earth System Model version 2, namely Community Atmosphere Model version 6  
232 (CAM6) coupled to Community Land Model (CLM) version 5.0 (Danabasolu et al. 2020). Five  
233 ensemble members are generated for each experiment by altering the initial atmospheric  
234 temperatures by the order of  $10^{-14}$  K (Kay *et al.*, 2015).

235

236 For the two warming experiments, the prescribed SSTs contain three components: the observed  
237 seasonally-varying climatology, an idealized repeating ENSO cycle, and a linearly increasing  
238 ‘global warming’ SST pattern as described below. For the Control experiment, the prescribed  
239 SSTs are identical to those in the EP and noEP experiments except that the global warming trend  
240 component is omitted. For the EP and noEP experiments, atmospheric radiative forcing follows

241 the SSP5-85 scenario and in the Control experiment, atmospheric radiative forcing conditions are  
242 fixed at year 2000 levels. As such, the Control experiment provides a baseline climatology from  
243 which effects due to both the Pacific warming pattern and global warming can be distinguished.

244

245 The linearly increasing global warming component is obtained by calculating the SST trend over  
246 the period 2015-2100 from a fully coupled simulation of CESM1 under the RCP 8.5 emissions  
247 scenario. We use this pattern as representative of a typical CMIP SST warming pattern in  
248 response to global warming (Heede and Fedorov, 2021), where the eastern tropical Pacific  
249 warms more than other tropical ocean regions. We refer to the first experiment as **EP** (enhanced  
250 eastern tropical Pacific warming) in which the eastern equatorial warming pattern from the  
251 original experiment is retained (Fig. 1a). The second experiment is called **noEP** (no eastern  
252 tropical Pacific enhanced warming), in which the eastern equatorial Pacific warming signal is  
253 replaced by a uniform tropical warming pattern (Fig. 1b). All trends are linear in time, so that the  
254 magnitudes of the patterns in Figs. 1a and 1b increase by a fixed amount at each time step over  
255 the years 2015-2100 (as illustrated in Fig. 1d). While the two experiments differ in how much the  
256 tropical Pacific warms, they are virtually identical in their global mean climate sensitivity, and  
257 hence the response in the hydrological cycle can be considered a direct response to the different  
258 patterns of warming rather than a response to differing rates of global warming.

259

260 While other studies using dynamically coupled ocean pacemaker experiments (Zhang *et al.*,  
261 2019) are designed to obtain the most realistic response to a given regional SST anomaly pattern,  
262 our modeling framework is meant to isolate the terrestrial precipitation impacts strictly in  
263 response to tropical Pacific SST warming patterns. Therefore, we have designed our experiments

264 so that only SST patterns in the tropical Pacific are altered while SSTs in the remaining ocean  
265 basins are unchanged (e.g., the so-called Tropical Ocean – Global Atmosphere TOGA set-up; see  
266 for example(Deser *et al.*, (2017)). While this approach does not allow us to investigate the  
267 dynamical ocean response to the imposed SST anomaly, it does allow us to isolate the  
268 precipitation response directly arising from changes in the tropical Pacific and not from  
269 secondary effects of other ocean warming patterns formed in response to the imposed SST. As  
270 such, our experiments should be considered a sensitivity experiment answering the question:  
271 Does the projected tropical Pacific warming pattern and its interaction with the ENSO cycle  
272 matter for terrestrial hydroclimate change?

273

#### 274 *2.1.1 Idealized ENSO cycle*

275 The prescribed idealized ENSO cycle is amplitude-symmetric and consists of one strong and one  
276 weak El Niño and La Niña per decade (Fig. 1d-e). Each prescribed idealized ENSO event  
277 follows a gaussian function lasting exactly one year with a peak in December, similar to typical  
278 ENSO events in observations. Strong and weak idealized ENSO events correspond to maximum  
279 Niño3.4 anomalies of approximately  $\pm 2$  and  $\pm 1$  °C, respectively. The spatial pattern of ENSO is  
280 obtained from the leading global EOF of detrended SSTs during 1950-2020 from the ERSSTv5  
281 (Huang *et al.*, 2017) instrumental reconstruction (Fig. 1c). The seasonal SST climatology is  
282 based on the HadISST gridded reconstruction from 1982-2002 (Rayner *et al.*, 2003).

283

284 Our motivation for imposing this highly idealized ENSO cycle is to isolate strictly the effects of  
285 the superposition of ENSO-like interannual SST variations on a varying background state  
286 without considering changes to ENSO itself. If we attempted to mimic a more realistic ENSO

287 cycle including, for example, weaker but longer lasting La Nina events, and eastern Pacific  
288 versus central Pacific events, it would be difficult to distinguish the effects on terrestrial  
289 hydroclimates arising from the ENSO background superposition from changes to the ENSO  
290 cycle itself without an excessively large number of ensemble members. As such, the goal of  
291 imposing an idealized ENSO cycle onto the EP and noEP experiments is to conduct a sensitivity  
292 study investigating how sensitive ENSO teleconnections are to a change in the background state,  
293 and as such should not be regarded as an attempt to be as realistic as possible.

294

## 295 *2.2 Analysis methods*

296 In order to highlight how tropical Pacific warming patterns affect the hydroclimate in the  
297 Americas, we apply the following analysis to the EP and noEP experiments:

298 1) For each grid cell and each ensemble member, we calculate the linear trends over the  
299 period 2015-2100 for precipitation (combined large-scale and convective), sea level  
300 pressure (SLP) and 250mb and 850mb winds for all months. We then mask out all grid  
301 cells where all 5 ensemble members do not agree on the sign of the trend. Next, we  
302 compute the difference between the ensemble averages of the EP and noEP experiments  
303 and conduct a Student t-test for each grid cell and mask out grid cells where the  
304 differences are not statistically different at the 95% confidence interval using all 5  
305 ensemble members.

306 2) To highlight the underlying large-scale dynamics driving changes in terrestrial  
307 precipitation, we next compute trends in upper-levels wind divergence (250 mb)  
308 following the same procedure as in 1) to illustrate spatial changes in tropical convection  
309 between the EP and noEP experiments. Next, we calculate integrated water vapor

310 divergence to illustrate how changes in moisture divergence drive the observed changes  
 311 in precipitation. The integrated moisture divergence  $\nabla \cdot Q$  is calculated on monthly  
 312 output following Trenberth and Guillemot (1998) and Xu *et al.* (2016):

$$313 \quad \nabla \cdot Q = \nabla \cdot \frac{1}{g} \int_{P_{min}}^{P_s} q \mathbf{v} dp$$

314  
 315 Where  $q$  is specific humidity,  $\mathbf{v}$  is the horizontal velocity vector,  $g$  is the gravitational  
 316 constant,  $P_s$  is 1000 mb, and  $P_{min}$  is 25 mb. We then evaluate the trends over time of  
 317 moisture divergence  $\nabla \cdot Q$  following same procedure as step 1).

318

319 3) We select 5 regions of interest in which we conduct a regional hydroclimate analysis.

320 Three regions are selected visually from step 1) as regions that have a statistically  
 321 significant precipitation trend between the EP and noEP experiments (Southern Mexico,  
 322 Central America, Central Amazon and South-Eastern South America). An additional 2  
 323 regions, U.S. West coast and Southern Chile are selected based on differences between  
 324 the two experiments with regards to extreme precipitation (see section 4). The regional  
 325 extent of the 5 regions are as follows:

326 a. U.S. West Coast (236° E to 240° E, 36° N to 47° N)

327 b. Southern Mexico (255° E to 265° E, 25° N to 25° N)

328 c. Central America (272° E to 282° E, 19° N to 20° N)

329 d. Central Amazon (295° E to 315° E, 10° S to 0° N)

330 e. South-Central South America (300° E to 315° E, 32° S to 17° S)

331 f. Southern Chile (283° E to 288° E, 55° S to 45° S)

332

333 Precipitation trends are averaged spatially within these regions, and a histogram is  
334 computed for 12-month smoothed timeseries across all 5 ensemble members of the EP,  
335 noEP and Control experiments to illustrate differences in the annual distributions  
336 between the EP and noEP experiments relative to the control experiment. Next, a 10-year  
337 smoothed time series is plotted to illustrate trends over time. Finally, trends are computed  
338 for each month of the year to illustrate the seasonal manifestation of the differences  
339 between the EP and noEP experiments and these are compared with the climatology from  
340 the Control experiment.

341  
342 4) We quantify how the mean state of the tropical Pacific affects the distribution of end-of-  
343 century (2050-2100) boreal winter (DJFM) precipitation in the five regions of interest. As  
344 before, we determine anomalies in both the EP and noEP runs relative to the control  
345 climatology—not, say, relative to an earlier period within the EP and noEP runs. The  
346 empirical distribution of regional rainfall is then calculated over El Niño, La Niña, and  
347 neutral years, 2050-2100. We choose a 50-year period to improve estimates of the  
348 distribution as the results are qualitatively similar for shorter end-of-century periods.

349  
350 5) We then compare these end-of-century distributions to extreme quantiles from the control  
351 simulation to determine the role of the tropical Pacific mean state on seasonal extremes  
352 under global warming. Extreme dry and wet seasons are defined as the 2.5<sup>th</sup> and 97.5<sup>th</sup>  
353 percentiles of the DJFM regional precipitation in the control simulation calculated across  
354 all years and therefore all ENSO phases. The proportion of seasons with end-of-century

355 seasonal extreme precipitation is thus calculated as the ratio of seasons exceeding this  
356 threshold over the total number of seasons.

357

### 358 **3. Results**

#### 359 *3.1 21<sup>st</sup> century precipitation trends in the Americas*

360 The two experiments, noEP and EP, have broadly similar patterns of changes in precipitation and  
361 large-scale circulation (Fig. 2). In particular, the wetting along the west coast of Canada, Alaska,  
362 and central Argentina, and the drying trends in southern Mexico and Central America as well as  
363 the central Amazon region are robust responses to global warming that are relatively insensitive  
364 to the pattern of warming in the eastern tropical Pacific Ocean. However, there are some crucial  
365 differences between the two experiments (Fig. 2c) – namely a stronger drying trend along the  
366 Pacific coast of southern Mexico and Central America, and the Amazon region, in response to  
367 enhanced eastern Pacific warming. Meanwhile the edges of this deep tropical drying trend shift  
368 equatorward, such that the continental United States and subtropical South America are wetter on  
369 average in the EP experiment compared to noEP. In other words, in the noEP experiment, the  
370 drying trends extend farther poleward, while in the EP experiment, the drying trend is intensified  
371 in the deep tropics.

372

373 While the Aleutian Low in the north Pacific is intensified in both warming experiments, it is  
374 intensified much more and shifted further eastward in EP compared to noEP (Fig. 2c). In the  
375 Southern Hemisphere midlatitudes, positive SLP anomalies are observed in both experiments,  
376 but in the EP experiment an intensification and eastward shift of the anticyclonic trend centered  
377 on the southern tip of South America is apparent (Fig 2b). Despite changes in extra-tropical SLP

378 patterns, the long-term trends in terrestrial precipitation are generally not statistically different  
379 between the two experiments beyond latitudes of 30° N and 30° S.

380  
381 To understand the dynamics driving exacerbated drying trends in the tropical American regions  
382 in the EP experiment, we examine the trends in moisture divergence and upper-level wind  
383 divergence (Figs. 3-4). The easterly trades in the tropical Pacific weaken in both experiments  
384 (Fig 3). This weakening is amplified in the EP experiment, resulting in a greater eastward shift of  
385 the Walker cell with anomalous deep convection (Fig. 4c) and moisture convergence (Fig 3c) in  
386 the central Pacific, and anomalous moisture divergence over the Maritime continent, Central  
387 America and the Amazon region. Furthermore, an anomalous divergence of upper-level winds in  
388 the central Pacific and a convergence of upper-level winds in the Amazon region is observed,  
389 which acts to suppress convection and precipitation in this region (Fig 4c).

390  
391 Not surprisingly, these differences in circulation and precipitation trends over the Americas  
392 between the EP and noEP experiments largely resemble the pattern of anomalies observed during  
393 El Niño events (Lenssen et al. 2020). Importantly, however, these trends appear as long-term  
394 trends averaged across all months and all phases of ENSO, enabling us to evaluate the statistics  
395 of hydrological changes in all seasons. The following section describes the projected regional  
396 hydroclimate changes over the Americas and their dependence on the pattern of warming in the  
397 eastern Pacific in more detail.

398

399

400

### 401 3.2 Regional and seasonal precipitation trends across the Americas

402 Both south-central Mexico and Central America experience a shift in annual precipitation  
403 towards drier conditions (Fig. 5) which is exacerbated in the EP experiment, but the seasonality  
404 of changes differs across these regions illustrating the interaction between the long-term Pacific  
405 warming trend and the mean climatology. In southern Mexico, the difference between EP and the  
406 noEP experiments is manifested primarily in October and November (Fig. 5c), while for Central  
407 America, the changes span the full calendar year (Fig. 5d). The central Amazon region is notable  
408 since the difference between the EP and noEP experiments is evident both as a mean shift  
409 towards drier conditions and a significant increase in extreme dry years in the EP experiment.  
410 For this region, the difference between the experiments is greatest in the February through  
411 August (Fig. 6f). In southeastern South America, the difference between EP and noEP is  
412 opposite with a long-term drought trend emerging in the noEP experiment, but not in the EP  
413 experiment, reflecting the equatorward shift of drying trends described in section 3.1.

414  
415 Along the US west coast (Fig. 5a) and in southern Chile (Fig. 6g), differences between the EP  
416 and noEP experiment are not evident in the mean trend. However, in the US west coast region,  
417 the EP experiment results in more wet year extremes compared with the noEP experiment (Fig.  
418 5a) whereas for southern Chile, the EP experiment results in more dry year extremes compared  
419 with the noEP experiment (Fig. 6i).

420

### 421 3.3 Changes in extreme precipitation stratified by ENSO phase

422 Next, we focus on the projected changes in extreme precipitation (defined as the frequency of  
423 events exceeding the 95<sup>th</sup> percentile of the Control simulation) in the two warming experiments

424 during the DJFM and their dependence on ENSO phase. We are focusing on DJFM in this  
425 section because the ENSO signal is strongest during this time. Fig. 7 shows that the frequency of  
426 wet extremes during DJFM in Canada and Alaska occur in all 3 ENSO phases (Neutral, El Nino  
427 and La Nina). For the continental United States, however, wet extremes are more frequent during  
428 El Nino years than ENSO neutral years, and nearly absent during La Nina years. For Central  
429 America and the Amazon region, dry extremes occur almost exclusively during El Nino years.  
430 Conversely, wet extremes in the Amazon region occur during La Nina years.

431  
432 Fig. 8 shows the locations where there are statistically significant differences in extreme  
433 precipitation between the EP and noEP experiments for each ENSO phase. During ENSO neutral  
434 years, significant differences are limited to wet extremes over Canada, with fewer extreme wet  
435 winters in EP compared to noEP (Fig. 8a,b). Despite the imposed symmetry in the ENSO cycle,  
436 the largest significant differences in extreme precipitation between EP and noEP occur mainly  
437 during El Nino years, with more extreme dry DJFM seasons in the Amazon and Central  
438 American regions and fewer in South-Central South America (Figs. 8e,f). The EP experiment  
439 also leads to more wet extremes along the US West coast and less wet extremes in Arctic  
440 Canada. During La Nina years, the EP experiment causes fewer wet extremes in the Central  
441 Amazon region relative to the noEP experiment.

442  
443 To complement the spatial analysis, we examine future (2050-2100) changes in DJFM  
444 precipitation distributions during El Nino years vs. La Nina years in the EP and noEP  
445 experiments relative to the Control in each selected region (Fig. 9). Notably, we see that for the  
446 U.S. West Coast, the most prominent difference between the two warming experiments occurs

447 during El Niño years, with the EP experiment showing a shift toward more frequent wet  
448 extremes relative to the noEP experiment (compare solid orange vs. blue curves in Fig. 9a); La  
449 Nina years are relatively insensitive to the pattern of eastern tropical Pacific warming  
450 (comparing dashed orange vs. blue curves in Fig. 9a). For Central America, the EP experiment is  
451 drier than noEP in both La Nina and El Nino years (compare dashed and solid curves in Fig. 9b),  
452 but because El Nino years are generally drier than La Niña years, the dry extremes (relative to  
453 Control) are also more prominent during El Niño compared to La Nina. For the central Amazon  
454 region, the difference between the EP and noEP experiments is amplified during El Niño years,  
455 which accounts for the most extreme dry years. In two cases, the noEP experiment shifts El Nino  
456 conditions more than the EP experiment. In southern Mexico, there's a shift towards wetter  
457 extremes during El Nino years for the noEP experiment (Fig. 9b), while for south-central South  
458 America, there is a shift towards drier conditions during El Nino (Fig. 9e.). Southern Chile,  
459 however, shows a shift towards drier conditions during El Nino years in both the EP and noEP  
460 experiments, but with more dry extremes in the EP experiment (Fig. 9f).

461

462 Overall, these results show that, despite imposing ENSO symmetry in the SST forcing, most  
463 differences of precipitation extremes between the EP and noEP experiment occurs during El  
464 Nino events, illustrating how the background Pacific warming can modulate ENSO precipitation  
465 extremes without changes to ENSO amplitude itself.

466

#### 467 **4 Discussion**

468 This study has investigated how enhanced eastern equatorial Pacific SST warming projected by  
469 CMIP-class models (but not found in observations to date) significantly modulates future

470 precipitation trends and variability across the Americas using a set of idealized AGCM  
471 experiments with CAM6. Similar to El Niño, an increase in deep convection and moisture  
472 convergence in the Pacific caused by enhanced eastern Pacific warming drives moisture  
473 divergence from the tropical American regions and an anomalous convergence of moisture in the  
474 Atlantic at 30°N and 30°S. The resultant difference in the spatial patterns of precipitation trends  
475 in the Americas between the experiments with and without enhanced eastern Pacific warming  
476 (EP vs. noEP) is a contraction and intensification of tropical drying trends: southern Mexico,  
477 Central America and the central Amazon region become drier on average in the EP experiment,  
478 while the continental US and the south-central part of South America become wetter. The  
479 differences in precipitation manifest heterogeneously seasonally and spatially. For instance, the  
480 difference between EP and noEP in Central America manifests as a year-round shift of the full  
481 distribution whereas differences in southern Mexico differences are largest in October and  
482 November, and in the central Amazon region the differences are largest in February through  
483 August.

484  
485 In addition to driving long-term changes in mean precipitation, the EP and noEP warming  
486 experiments also modulate extreme precipitation, especially during El Niño years. For example,  
487 dry extremes during El Niño are exacerbated greatly in Central America and the central Amazon  
488 region in the EP experiment, while they are reduced in south-central South America (southern  
489 Brazil, Paraguay, Uruguay, and northern Argentina). This illustrates that the superposition of the  
490 ENSO cycle with different background warming patterns in the tropical Pacific can modulate the  
491 occurrence of extreme precipitation events over land, even in the absence of changes in ENSO  
492 amplitude.

493

494 These results are qualitatively similar to previous multi-model studies of forced hydroclimate  
495 trends (Seager and Vecchi, 2010; Watterson, 2023) and of forced changes to ENSO  
496 teleconnections (Beverley *et al.*, 2021; O'Brien and Deser, 2022), suggesting that the findings  
497 are not specific to our chosen AGCM. However, known biases in simulating convective and  
498 large-scale precipitation in AGCMs should be kept in mind when evaluating these results.

499

500 The idealized ENSO cycle prescribed in our study was chosen to evaluate the effect of the mean  
501 state change on ENSO teleconnections in the absence of changes to ENSO variability itself.  
502 Therefore, by design, it does not sample the full range of potential historical and projected ENSO  
503 events (Maher et al. 2023), including ENSO asymmetry and diversity (Capotondi *et al.*, 2015),  
504 and multi-year ENSO events (Okumura, DiNezio and Deser, 2017; Sanchez and Karneuskas,  
505 2021). Thus, a complete range of potential future ENSO related impacts cannot be gauged from  
506 our experimental design. Yet, the simplicity of our design allows us to isolate how ENSO  
507 interacts with the mean state in future warming scenarios. This provides a basis for future studies  
508 evaluating extreme events associated with other changing ENSO characteristics, perhaps  
509 complemented by pacemaker experiments.

510

511 Our findings have important implications for adaptation and mitigation considerations, as the  
512 presence or absence of enhanced eastern Pacific warming in the 21<sup>st</sup> century influences the  
513 severity and location of droughts and changes the distribution of extreme precipitation events in  
514 complex ways. By design, the EP and noEP experiments are constrained to be identical except  
515 for their tropical Pacific warming patterns; thus, we have used a “climate storyline” approach,

516 that explicitly considers potential uncertainties and systematic model biases in the response of  
517 the physical climate system to greenhouse gas forcing (Shepherd, 2019). We suggest this  
518 approach be used in regions beyond the Americas to better represent the full range of uncertainty  
519 in future tropical Pacific-driven changes in hydroclimate. The method can also be applied to  
520 understand the impacts of warming patterns in other ocean basins.

521  
522 Our findings tell a cautionary tale about relying on multi-model ensemble projections to  
523 understand the full range of regional precipitation responses to global warming, particularly  
524 when the ensemble is not in agreement with the observed system. Hence, we have illustrated the  
525 pressing importance of improving simulations of the coupled ocean-atmosphere response to  
526 anthropogenic forcing as well as better understanding uncertainties in climate impacts not  
527 reflected in the spread of IPCC-class models.

528

529

### 530 **Acknowledgements and funding sources**

531

532 This research is funded by the Corporative Institute for Research in the Environmental Sciences  
533 (CIRES) Visiting Fellowship Program. We further acknowledge Adam Phillips at National  
534 Center for Atmospheric Research for assistance with computational experiments as well as  
535 NCAR CISL grants UCUB0127, UCUB0131, UCUB0127 and UCUB0141. Publication of this  
536 article was funded by the University of Colorado Boulder Libraries Open Access Fund. The  
537 National Center for Atmospheric Research is sponsored by the National Science Foundation.

538

539

540 **Data availability**

541 All model experiments will be made publicly available upon publication via the National Center  
542 for Atmospheric Research. All code used for analysis and visualization will be made available  
543 via GitHub upon publication.

544

545

546 **4 References**

547

548 Allen, M.R. and Ingram, W.J. (2002) ‘Constraints on future changes in climate and the  
549 hydrologic cycle’, *Nature*, 419(6903), pp. 224–232. Available at:  
550 <https://doi.org/10.1038/nature01092>.

551 Beverley, J.D. *et al.* (2021) ‘Future changes to El Niño teleconnections over the north Pacific  
552 and North America’, *Journal of Climate*, 34(15), pp. 6191–6205.

553 Bjerknes, J. (1969) ‘Atmospheric teleconnections from the equatorial Pacific’, *Monthly weather  
554 review*, 97(3), pp. 163–172.

555 Bloch-Johnson, J. *et al.* (2024) ‘The Green’s Function Model Intercomparison Project (GFMIIP)  
556 Protocol’, *Journal of Advances in Modeling Earth Systems*, 16(2), p. e2023MS003700. Available  
557 at: <https://doi.org/10.1029/2023MS003700>.

558 Bonfils, C.J. *et al.* (2015) ‘Relative contributions of mean-state shifts and ENSO-driven  
559 variability to precipitation changes in a warming climate’, *Journal of Climate*, 28(24), pp. 9997–  
560 10013.

561 Buchwald, A.G. *et al.* (2022) ‘The Association Between Rainfall, Temperature, and Reported  
562 Drinking Water Source: A Multi-Country Analysis’, *GeoHealth*, 6(11), p. e2022GH000605.  
563 Available at: <https://doi.org/10.1029/2022GH000605>.

564 Cai, W. *et al.* (2022) ‘Increased ENSO sea surface temperature variability under four IPCC  
565 emission scenarios’, *Nature Climate Change*, 12(3), pp. 228–231. Available at:  
566 <https://doi.org/10.1038/s41558-022-01282-z>.

567 Capotondi, A. *et al.* (2015) ‘Understanding ENSO Diversity’, *Bulletin of the American  
568 Meteorological Society*, 96(6), pp. 921–938. Available at: [https://doi.org/10.1175/BAMS-D-13-  
569 00117.1](https://doi.org/10.1175/BAMS-D-13-00117.1).

570 Chou, C. and Neelin, J.D. (2004) ‘Mechanisms of Global Warming Impacts on Regional  
571 Tropical Precipitation’, *Journal of Climate*, 17(13), pp. 2688–2701. Available at:  
572 [https://doi.org/10.1175/1520-0442\(2004\)017<2688:MOGWIO>2.0.CO;2](https://doi.org/10.1175/1520-0442(2004)017<2688:MOGWIO>2.0.CO;2).

- 573 Clement, A.C. *et al.* (1996) ‘An ocean dynamical thermostat’, *Journal of Climate*, 9(9), pp.  
574 2190–2196.
- 575 Crochemore, L., Ramos, M.-H. and Pappenberger, F. (2016) ‘Bias correcting precipitation  
576 forecasts to improve the skill of seasonal streamflow forecasts’, *Hydrology and Earth System  
577 Sciences*, 20(9), pp. 3601–3618. Available at: <https://doi.org/10.5194/hess-20-3601-2016>.
- 578 Deser, C. *et al.* (2017) ‘The Northern Hemisphere Extratropical Atmospheric Circulation  
579 Response to ENSO: How Well Do We Know It and How Do We Evaluate Models  
580 Accordingly?’, *Journal of Climate*, 30(13), pp. 5059–5082. Available at:  
581 <https://doi.org/10.1175/JCLI-D-16-0844.1>.
- 582 Devereux, S. (2007) ‘The impact of droughts and floods on food security and policy options to  
583 alleviate negative effects’, *Agricultural Economics*, 37(s1), pp. 47–58. Available at:  
584 <https://doi.org/10.1111/j.1574-0862.2007.00234.x>.
- 585 DiNezio, P., Clement, A. and Vecchi, G. (2010) ‘Reconciling Differing Views of Tropical  
586 Pacific Climate Change’, *Eos, Transactions American Geophysical Union*, 91(16), pp. 141–142.  
587 Available at: <https://doi.org/10.1029/2010EO160001>.
- 588 Dong, B. and Lu, R. (2013) ‘Interdecadal enhancement of the Walker circulation over the  
589 tropical Pacific in the late 1990s’, *Advances in Atmospheric Sciences*, 30(2), pp. 247–262.
- 590 Dong, Y. *et al.* (2019) ‘Attributing Historical and Future Evolution of Radiative Feedbacks to  
591 Regional Warming Patterns using a Green’s Function Approach: The Preeminence of the  
592 Western Pacific’. Available at: <https://doi.org/10.1175/JCLI-D-18-0843.1>.
- 593 Dong, Y. *et al.* (2022) ‘Two-way teleconnections between the Southern Ocean and the tropical  
594 Pacific via a dynamic feedback’, *Journal of Climate*, 35(19), pp. 2667–2682.
- 595 Fosu, B., He, J. and Liguori, G. (2020) ‘Equatorial Pacific Warming Attenuated by SST  
596 Warming Patterns in the Tropical Atlantic and Indian Oceans’, *Geophysical Research Letters*,  
597 47(18), p. e2020GL088231. Available at: <https://doi.org/10.1029/2020GL088231>.
- 598 Fredriksen, H.-B. *et al.* (2020) ‘How Does El Niño–Southern Oscillation Change Under Global  
599 Warming—A First Look at CMIP6’, *Geophysical Research Letters*, 47(22), p. e2020GL090640.  
600 Available at: <https://doi.org/10.1029/2020GL090640>.
- 601 Greve, P. *et al.* (2014) ‘Global assessment of trends in wetting and drying over land’, *Nature  
602 Geoscience*, 7(10), pp. 716–721. Available at: <https://doi.org/10.1038/ngeo2247>.
- 603 Gulev, S.K. *et al.* (2021) ‘Chapter 2: Changing State of the Climate System’, in V. Masson-  
604 Delmotte *et al.* (eds) *Climate Change 2021: The Physical Science Basis. Contribution of  
605 Working Group I to the Sixth Assessment Report of the Intergovernmental Panel on Climate  
606 Change*. Cambridge, United Kingdom and New York, NY, USA: Cambridge University Press,  
607 Cambridge.

- 608 Harp, R.D. *et al.* (2021) ‘Interannual Climate Variability and Malaria in Mozambique’,  
609 *GeoHealth*, 5(2), p. e2020GH000322. Available at: <https://doi.org/10.1029/2020GH000322>.
- 610 He, C. and Li, T. (2019) ‘Does global warming amplify interannual climate variability?’, *Climate*  
611 *Dynamics*, 52(5), pp. 2667–2684. Available at: <https://doi.org/10.1007/s00382-018-4286-0>.
- 612 Heede, U. and Fedorov, A. (2021) ‘Eastern equatorial Pacific warming delayed by aerosols and  
613 thermostat response to CO<sub>2</sub>’.
- 614 Heede, U.K. and Fedorov, A.V. (2023a) ‘Colder Eastern Equatorial Pacific and Stronger Walker  
615 Circulation in the Early 21st Century: Separating the Forced Response to Global Warming From  
616 Natural Variability’, *Geophysical Research Letters*, 50(3), p. e2022GL101020. Available at:  
617 <https://doi.org/10.1029/2022GL101020>.
- 618 Heede, U.K. and Fedorov, A.V. (2023b) ‘Towards understanding the robust strengthening of  
619 ENSO and more frequent extreme El Niño events in CMIP6 global warming simulations’,  
620 *Climate Dynamics*, 61(5), pp. 3047–3060. Available at: [https://doi.org/10.1007/s00382-023-](https://doi.org/10.1007/s00382-023-06856-x)  
621 06856-x.
- 622 Heede, U.K., Fedorov, A.V. and Burls, N.J. (2020) ‘Timescales and mechanisms for the Tropical  
623 Pacific response to global warming: a tug of war between the Ocean Thermostat and weaker  
624 Walker’, *Journal of Climate* [Preprint]. Available at: <https://doi.org/10.1175/JCLI-D-19-0690.1>.
- 625 Held, I.M. and Soden, B.J. (2006) ‘Robust responses of the hydrological cycle to global  
626 warming’, *Journal of climate*, 19(21), pp. 5686–5699.
- 627 Hong, Y., Adler, R. and Huffman, G. (2007) ‘Use of satellite remote sensing data in the mapping  
628 of global landslide susceptibility’, *Natural Hazards*, 43(2), pp. 245–256. Available at:  
629 <https://doi.org/10.1007/s11069-006-9104-z>.
- 630 Hu, S. and Fedorov, A.V. (2019) ‘Indian Ocean warming can strengthen the Atlantic meridional  
631 overturning circulation’, *Nature Climate Change*, 9(10), pp. 747–751. Available at:  
632 <https://doi.org/10.1038/s41558-019-0566-x>.
- 633 Huang, B. *et al.* (2017) ‘NOAA extended reconstructed sea surface temperature (ERSST),  
634 version 5’, *NOAA National Centers for Environmental Information*, 30, pp. 8179–8205.
- 635 Hwang, Y.-T. *et al.* (2024) ‘Contribution of anthropogenic aerosols to persistent La Niña-like  
636 conditions in the early 21st century’, *Proceedings of the National Academy of Sciences*, 121(5),  
637 p. e2315124121. Available at: <https://doi.org/10.1073/pnas.2315124121>.
- 638 Kang, S.M. *et al.* (2023) ‘Disentangling the mechanisms of equatorial Pacific climate change’,  
639 *Science Advances*, 9(19), p. eadf5059. Available at: <https://doi.org/10.1126/sciadv.adf5059>.
- 640 Kay, J.E. *et al.* (2015) ‘The Community Earth System Model (CESM) large ensemble project: A  
641 community resource for studying climate change in the presence of internal climate variability’,  
642 *Bulletin of the American Meteorological Society*, 96(8), pp. 1333–1349.

- 643 Keil, P. *et al.* (2020) ‘Multiple drivers of the North Atlantic warming hole’, *Nature Climate*  
644 *Change*, 10(7), pp. 667–671. Available at: <https://doi.org/10.1038/s41558-020-0819-8>.
- 645 Kosaka, Y. and Xie, S.-P. (2013) ‘Recent global-warming hiatus tied to equatorial Pacific  
646 surface cooling’, *Nature*, 501(7467), pp. 403–407. Available at:  
647 <https://doi.org/10.1038/nature12534>.
- 648 Kotz, M., Levermann, A. and Wenz, L. (2022) ‘The effect of rainfall changes on economic  
649 production’, *Nature*, 601(7892), pp. 223–227. Available at: [https://doi.org/10.1038/s41586-021-](https://doi.org/10.1038/s41586-021-04283-8)  
650 04283-8.
- 651 Lenssen, N.J.L. *et al.* (2019) ‘Improvements in the GISTEMP Uncertainty Model’, *Journal of*  
652 *Geophysical Research: Atmospheres*, 124(12), pp. 6307–6326. Available at:  
653 <https://doi.org/10.1029/2018JD029522>.
- 654 Lenssen, N.J.L., Goddard, L. and Mason, S. (2020) ‘Seasonal Forecast Skill of ENSO  
655 Teleconnection Maps’, *Weather and Forecasting*, 35(6), pp. 2387–2406. Available at:  
656 <https://doi.org/10.1175/WAF-D-19-0235.1>.
- 657 Lesk, C., Coffel, E. and Horton, R. (2020) ‘Net benefits to US soy and maize yields from  
658 intensifying hourly rainfall’, *Nature Climate Change*, 10(9), pp. 819–822. Available at:  
659 <https://doi.org/10.1038/s41558-020-0830-0>.
- 660 Livneh, B. *et al.* (2024) ‘Can precipitation intermittency predict flooding?’, *Science of The Total*  
661 *Environment*, 945, p. 173824. Available at: <https://doi.org/10.1016/j.scitotenv.2024.173824>.
- 662 Maher, N. *et al.* (2023) ‘The future of the El Niño–Southern Oscillation: using large ensembles  
663 to illuminate time-varying responses and inter-model differences’, *Earth System Dynamics*,  
664 14(2), pp. 413–431. Available at: <https://doi.org/10.5194/esd-14-413-2023>.
- 665 Manabe, S. and Wetherald, R.T. (1975) ‘The Effects of Doubling the CO<sub>2</sub> Concentration on the  
666 climate of a General Circulation Model’, *Journal of the Atmospheric Sciences*, 32(1), pp. 3–15.  
667 Available at: [https://doi.org/10.1175/1520-0469\(1975\)032<0003:TEODTC>2.0.CO;2](https://doi.org/10.1175/1520-0469(1975)032<0003:TEODTC>2.0.CO;2).
- 668 Mason, S.J. and Goddard, L. (2001) ‘Probabilistic Precipitation Anomalies Associated with EN  
669 SO’, *Bulletin of the American Meteorological Society*, 82(4), pp. 619–638. Available at:  
670 [https://doi.org/10.1175/1520-0477\(2001\)082<0619:PPAAWE>2.3.CO;2](https://doi.org/10.1175/1520-0477(2001)082<0619:PPAAWE>2.3.CO;2).
- 671 Meehl, G.A., Wheeler, M. and Washington, W.M. (1994) ‘Low-frequency variability and CO<sub>2</sub>  
672 transient climate change. Part 3. Intermonthly and interannual variability’, *Climate Dynamics*,  
673 10(6), pp. 277–303. Available at: <https://doi.org/10.1007/BF00228028>.
- 674 Morice, C.P. *et al.* (2021) ‘An Updated Assessment of Near-Surface Temperature Change From  
675 1850: The HadCRUT5 Data Set’, *Journal of Geophysical Research: Atmospheres*, 126(3), p.  
676 e2019JD032361. Available at: <https://doi.org/10.1029/2019JD032361>.
- 677 Nadim, F. *et al.* (2006) ‘Global landslide and avalanche hotspots’, *Landslides*, 3(2), pp. 159–173.  
678 Available at: <https://doi.org/10.1007/s10346-006-0036-1>.

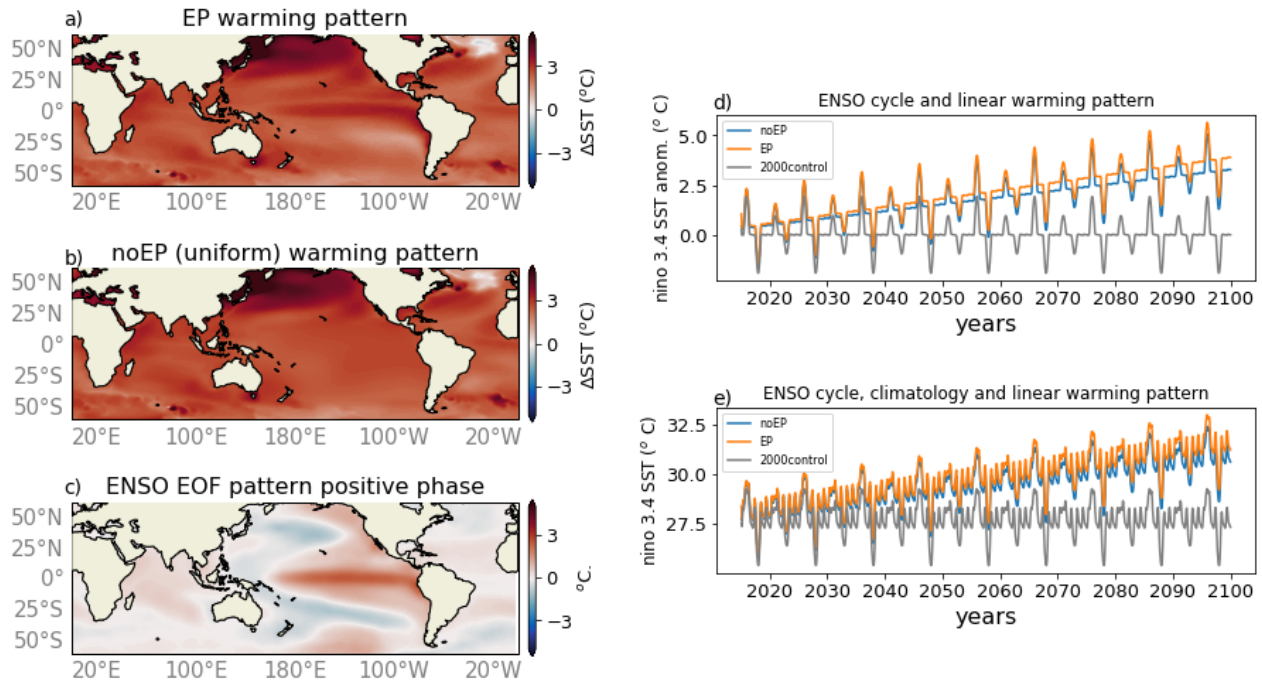
- 679 O'Brien, J.P. and Deser, C. (2022) 'Quantifying and Understanding Forced Changes to Unforced  
680 Modes of Atmospheric Circulation Variability over the North Pacific in a Coupled Model Large  
681 Ensemble', *Journal of Climate*, 36(1), pp. 19–37. Available at: <https://doi.org/10.1175/JCLI-D-22-0101.1>.
- 683 Okumura, Y.M., DiNezio, P. and Deser, C. (2017) 'Evolving Impacts of Multiyear La Niña  
684 Events on Atmospheric Circulation and U.S. Drought', *Geophysical Research Letters*, 44(22), p.  
685 11,614–11,623. Available at: <https://doi.org/10.1002/2017GL075034>.
- 686 Pendergrass, A.G. et al. (2017) 'Precipitation variability increases in a warmer climate',  
687 *Scientific Reports*, 7(1), p. 17966. Available at: <https://doi.org/10.1038/s41598-017-17966-y>.
- 688 Pfahl, S., O'Gorman, P.A. and Fischer, E.M. (2017) 'Understanding the regional pattern of  
689 projected future changes in extreme precipitation', *Nature Climate Change*, 7(6), pp. 423–427.  
690 Available at: <https://doi.org/10.1038/nclimate3287>.
- 691 Rayner, N.A. et al. (2003) 'Global analyses of sea surface temperature, sea ice, and night marine  
692 air temperature since the late nineteenth century', *Journal of Geophysical Research:  
693 Atmospheres*, 108(D14). Available at: <https://doi.org/10.1029/2002JD002670>.
- 694 Ropelewski, C.F. and Halpert, M.S. (1987) 'Global and Regional Scale Precipitation Patterns  
695 Associated with the El Niño/Southern Oscillation', *Monthly Weather Review*, 115(8), pp. 1606–  
696 1626. Available at: [https://doi.org/10.1175/1520-0493\(1987\)115<1606:GARSPP>2.0.CO;2](https://doi.org/10.1175/1520-0493(1987)115<1606:GARSPP>2.0.CO;2).
- 697 Sanchez, S.C. and Karnauskas, K.B. (2021) 'Diversity in the Persistence of El Niño Events Over  
698 the Last Millennium', *Geophysical Research Letters*, 48(18), p. e2021GL093698. Available at:  
699 <https://doi.org/10.1029/2021GL093698>.
- 700 Schwarzwald, K. et al. (2021) 'Changes in Future Precipitation Mean and Variability across  
701 Scales', *Journal of Climate*, 34(7), pp. 2741–2758. Available at: <https://doi.org/10.1175/JCLI-D-20-0001.1>.
- 703 Seager, R. et al. (2019) 'Strengthening tropical Pacific zonal sea surface temperature gradient  
704 consistent with rising greenhouse gases', *Nature Climate Change*, 9(7), pp. 517–522.
- 705 Seager, R., Henderson, N. and Cane, M. (2022) 'Persistent discrepancies between observed and  
706 modeled trends in the tropical Pacific Ocean', *Journal of Climate*, 1(aop), pp. 1–41. Available at:  
707 <https://doi.org/10.1175/JCLI-D-21-0648.1>.
- 708 Seager, R., Naik, N. and Vecchi, G.A. (2010) 'Thermodynamic and dynamic mechanisms for  
709 large-scale changes in the hydrological cycle in response to global warming', *Journal of climate*,  
710 23(17), pp. 4651–4668.
- 711 Seager, R. and Vecchi, G.A. (2010) 'Greenhouse warming and the 21st century hydroclimate of  
712 southwestern North America', *Proceedings of the National Academy of Sciences*, 107(50), pp.  
713 21277–21282. Available at: <https://doi.org/10.1073/pnas.0910856107>.

- 714 Shepherd, T.G. (2019) ‘Storyline approach to the construction of regional climate change  
715 information’, *Proceedings of the Royal Society A: Mathematical, Physical and Engineering  
716 Sciences*, 475(2225), p. 20190013. Available at: <https://doi.org/10.1098/rspa.2019.0013>.
- 717 Sun, D.-Z. and Liu, Z. (1996) ‘Dynamic ocean-atmosphere coupling: A thermostat for the  
718 tropics’, *Science*, 272(5265), pp. 1148–1150.
- 719 Trenberth, K.E. and Guillemot, C.J. (1998) ‘Evaluation of the atmospheric moisture and  
720 hydrological cycle in the NCEP/NCAR reanalyses’, *Climate Dynamics*, 14(3), pp. 213–231.  
721 Available at: <https://doi.org/10.1007/s003820050219>.
- 722 Vecchi, G.A. and Soden, B.J. (2007) ‘Global warming and the weakening of the tropical  
723 circulation’, *Journal of Climate*, 20(17), pp. 4316–4340.
- 724 Vicente-Serrano, S.M. et al. (2013) ‘Response of vegetation to drought time-scales across global  
725 land biomes’, *Proceedings of the National Academy of Sciences*, 110(1), pp. 52–57. Available at:  
726 <https://doi.org/10.1073/pnas.1207068110>.
- 727 Walker, G.T. (1925) ‘CORRELATION IN SEASONAL VARIATIONS OF WEATHER—A  
728 FURTHER STUDY OF WORLD WEATHER’, *Monthly Weather Review*, 53(6), pp. 252–254.  
729 Available at: [https://doi.org/10.1175/1520-0493\(1925\)53<252:CISVOW>2.0.CO;2](https://doi.org/10.1175/1520-0493(1925)53<252:CISVOW>2.0.CO;2).
- 730 Watanabe, M. et al. (2024) ‘Possible shift in controls of the tropical Pacific surface warming  
731 pattern’, *Nature*, 630(8016), pp. 315–324. Available at: <https://doi.org/10.1038/s41586-024-07452-7>.
- 733 Watanabe, T. et al. (2018) ‘Management of Climatic Extremes with Focus on Floods and  
734 Droughts in Agriculture’, *Irrigation and Drainage*, 67(1), pp. 29–42. Available at:  
735 <https://doi.org/10.1002/ird.2204>.
- 736 Watterson, I.G. (2023) ‘Atmospheric Moisture Transport Associated with Precipitation in  
737 Present and Simulated Future Climates’, *Journal of Climate*, 36(18), pp. 6409–6425.
- 738 Wetherald, R.T. and Manabe, S. (2002) ‘Simulation of hydrologic changes associated with  
739 global warming’, *Journal of Geophysical Research: Atmospheres*, 107(D19), p. ACL 7-1-ACL  
740 7-15. Available at: <https://doi.org/10.1029/2001JD001195>.
- 741 Wills, R.C.J. et al. (2022) ‘Systematic Climate Model Biases in the Large-Scale Patterns of  
742 Recent Sea-Surface Temperature and Sea-Level Pressure Change’, *Geophysical Research  
743 Letters*, 49(17), p. e2022GL100011. Available at: <https://doi.org/10.1029/2022GL100011>.
- 744 Wu, M. et al. (2021) ‘A very likely weakening of Pacific Walker Circulation in constrained near-  
745 future projections’, *Nature Communications*, 12(1), p. 6502. Available at:  
746 <https://doi.org/10.1038/s41467-021-26693-y>.
- 747 Xie, S.-P. et al. (2010) ‘Global warming pattern formation: Sea surface temperature and rainfall’,  
748 *Journal of Climate*, 23(4), pp. 966–986.

- 749 Xu, G. *et al.* (2016) ‘Different atmospheric moisture divergence responses to extreme and  
750 moderate El Niños’, *Climate Dynamics*, 47(1), pp. 393–410. Available at:  
751 <https://doi.org/10.1007/s00382-015-2844-2>.
- 752 Yeh, S.-W. *et al.* (2018) ‘ENSO Atmospheric Teleconnections and Their Response to  
753 Greenhouse Gas Forcing’, *Reviews of Geophysics*, 56(1), pp. 185–206. Available at:  
754 <https://doi.org/10.1002/2017RG000568>.
- 755 Ying, J. *et al.* (2022) ‘Emergence of climate change in the tropical Pacific’, *Nature Climate  
756 Change*, pp. 1–9. Available at: <https://doi.org/10.1038/s41558-022-01301-z>.
- 757 Yun, K.-S. *et al.* (2021) ‘Increasing ENSO–rainfall variability due to changes in future tropical  
758 temperature–rainfall relationship’, *Communications Earth & Environment*, 2(1), pp. 1–7.  
759 Available at: <https://doi.org/10.1038/s43247-021-00108-8>.
- 760 Zhang, L. *et al.* (2019) ‘Indian Ocean Warming Trend Reduces Pacific Warming Response to  
761 Anthropogenic Greenhouse Gases: An Interbasin Thermostat Mechanism’, *Geophysical  
762 Research Letters*, 46(19), pp. 10882–10890.
- 763 Zhou, Z.-Q. *et al.* (2014) ‘Global Warming–Induced Changes in El Niño Teleconnections over  
764 the North Pacific and North America’, *Journal of Climate*, 27(24), pp. 9050–9064. Available at:  
765 <https://doi.org/10.1175/JCLI-D-14-00254.1>.
- 766  
767  
768  
769  
770  
771  
772  
773  
774  
775  
776  
777  
778  
779  
780  
781  
782  
783  
784  
785  
786  
787  
788  
789

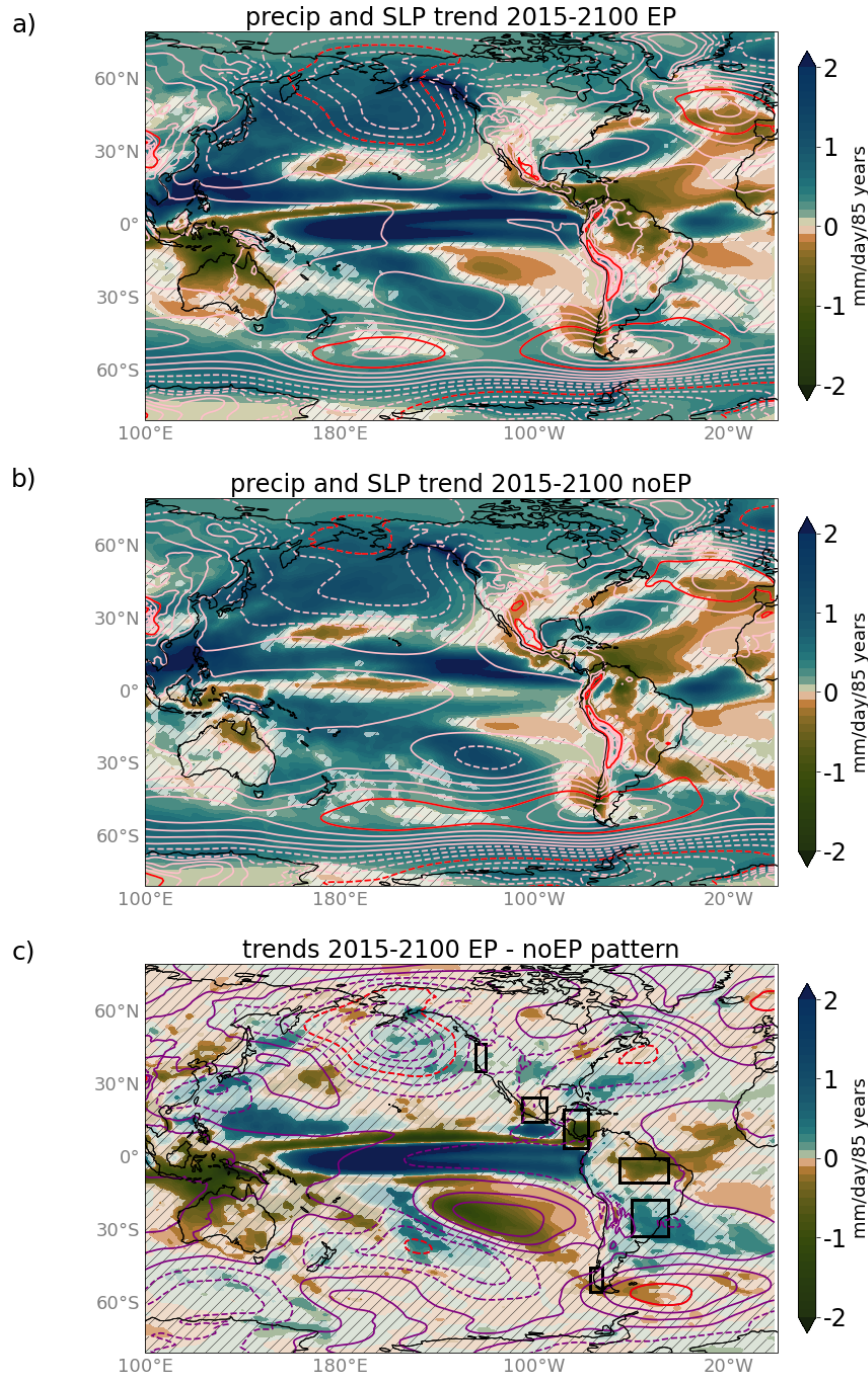
790 **5 Figures**

791  
792  
793



794  
795  
796  
797  
798  
799  
800  
801  
802  
803

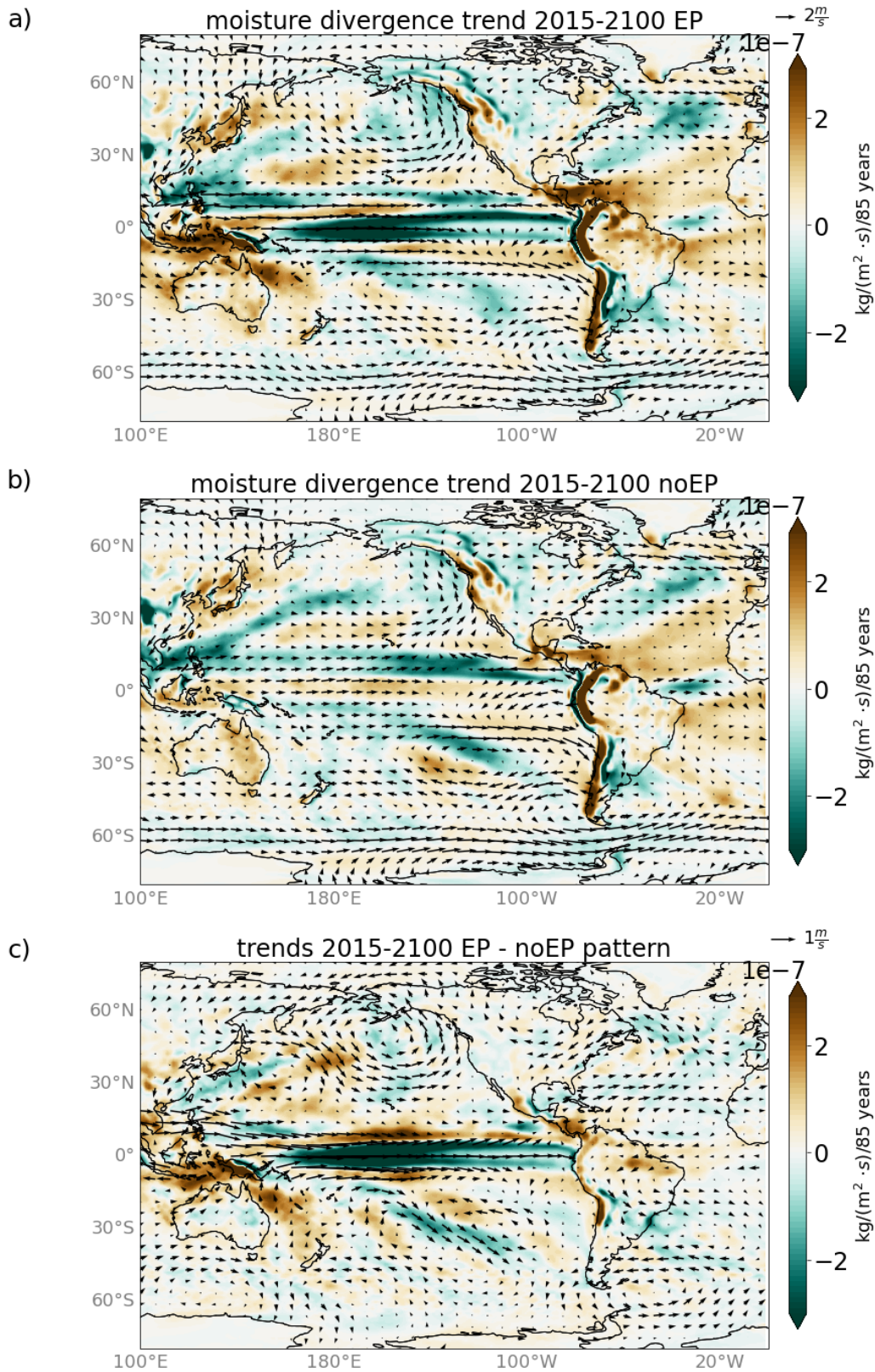
**Figure 1. EP and noEP warming patterns, and idealized ENSO cycle.** a) and b) SST anomalies averaged from 2080 to 2100 in the noEP and EP experiments, respectively. c) maximum positive phase of the EOF pattern applied in the idealized ENSO cycle. d) Niño3.4 SST timeseries in the EP (orange), noEP (blue) and 2000control (gray) experiments after removing the climatological seasonal cycle from the 2000control. e) same as d) but including the climatology



804  
805  
806  
807  
808  
809  
810  
811  
812  
813  
814

**Figure 2. Precipitation (color shading) and sea-level pressure (SLP; contours) trends from 2015-2100 based on all months for the a) EP experiment, b) noEP experiment and c) their difference (EP – noEP). Hatching in a) and b) indicates regions where not all ensemble members agree on the sign of the precipitation trend; hatching in c) indicates regions where the difference between the precipitation trends in the EP and noEP experiments is not statistically significant at the 95% confidence interval based on a Student’s t-test. The orange boxes indicate areas used for regional plots. In a) and b), the SLP contour interval is 0.50 hPa (negative values dashed, positive values solid) and the 2.00 hPa contours are highlighted in red. In c), the SLP contour interval is 0.25 hPa and the 0.75 hPa contours are highlighted in red.**

815



816  
817  
818

**Figure 3.** As in Fig. 2 but for column-integrated moisture divergence (color shading) and 850mb winds (vectors). In a) and b), the reference vector is 2 m/s and in c), the reference vector is 1 m/s.

819

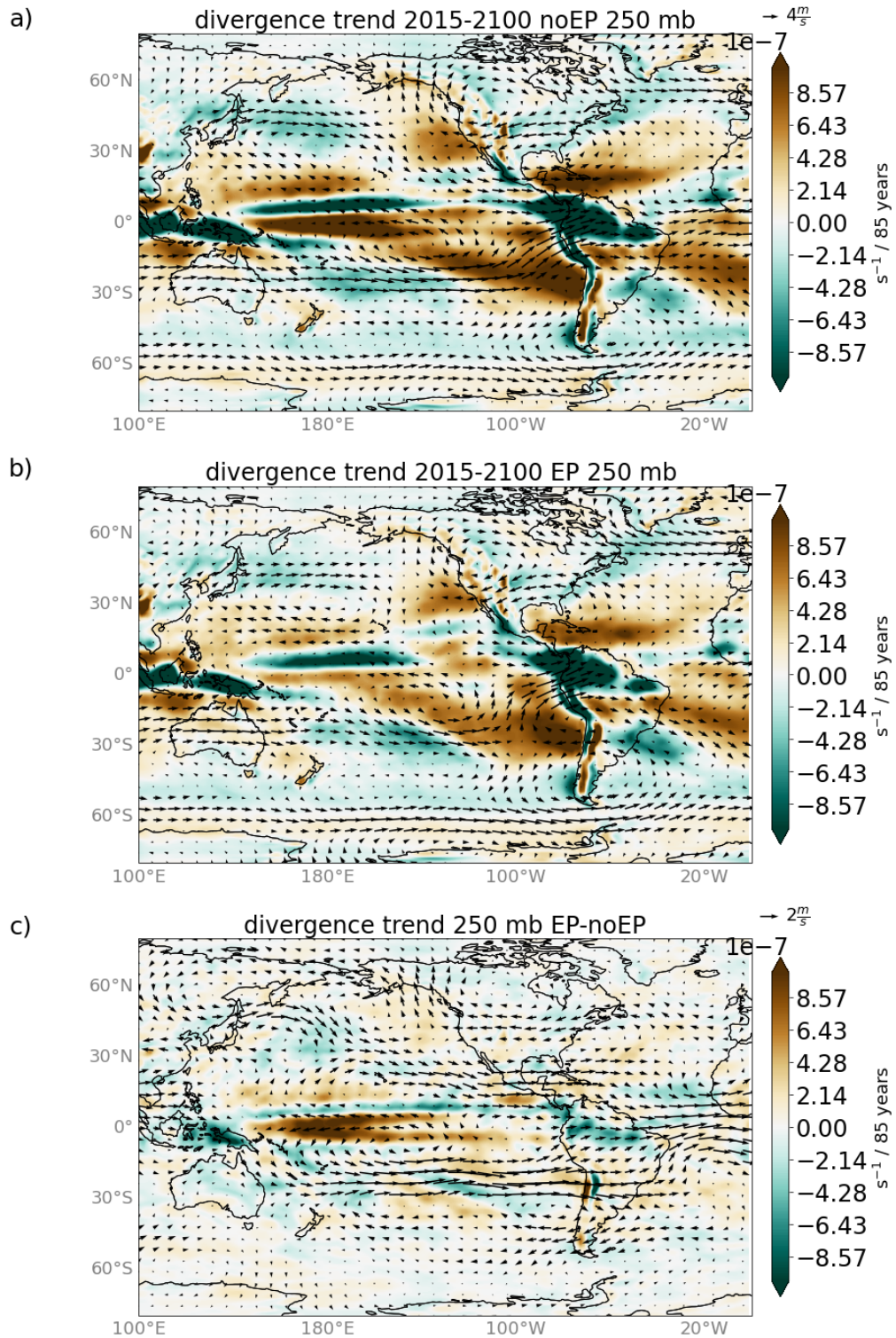
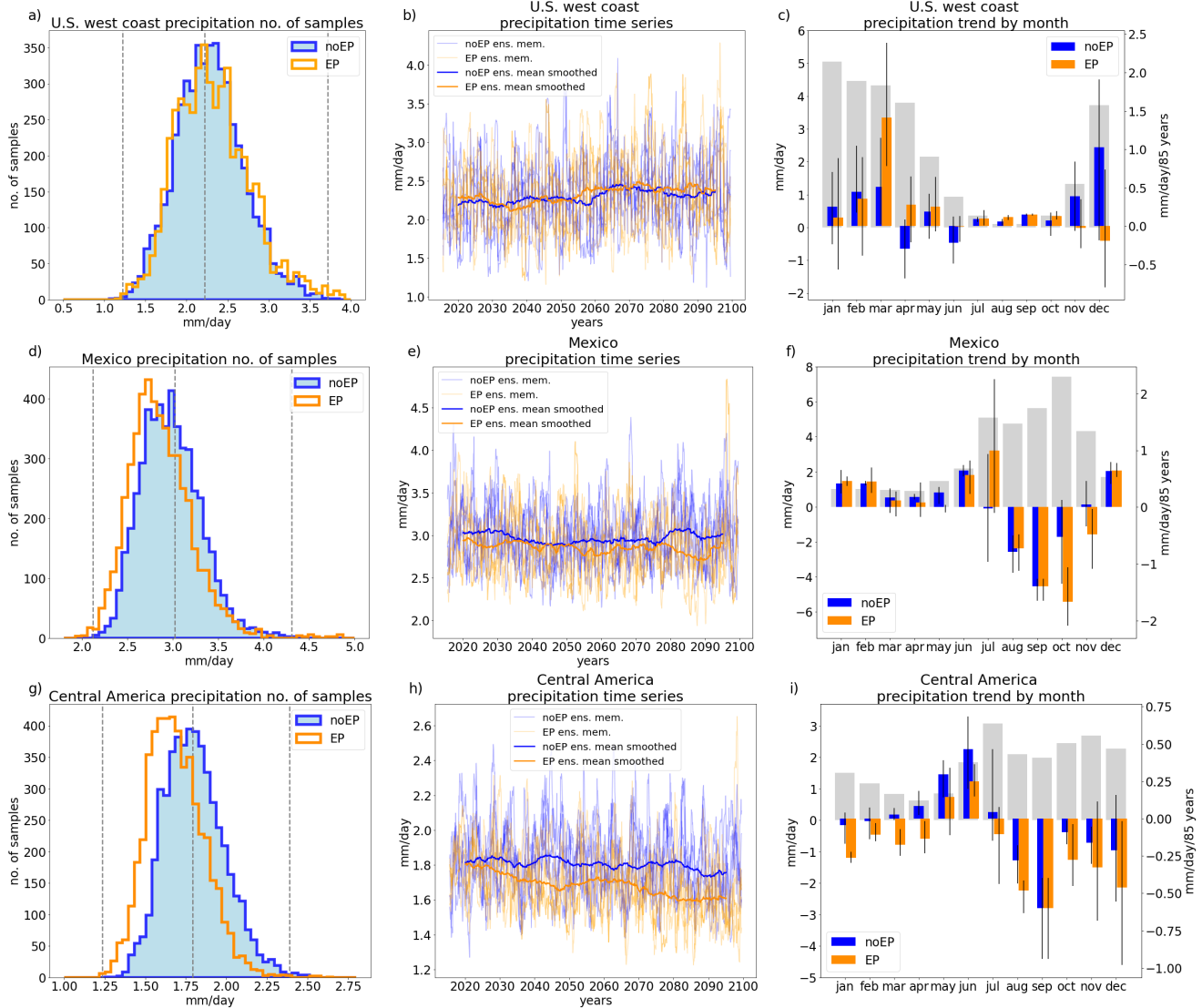


Figure 4. As in Fig. 2 but for upper level (250 mb) wind divergence (color shading) and 250mb winds (vectors) In a) and b), the reference vector is 4 m/s and in c) the reference vector is 2 m/s.

820  
821  
822  
823  
824  
825



826

827

828

829

830

831 **Figure 5. Regional overview of precipitation responses in the EP and noEP experiments for the U.S.**

832 **West Coast, Mexico and Central America (regions outlined in Fig. 1c). Left: histogram of monthly**

833 **precipitation from 2015 to 2100 (mm/day) after applying a 12-month running mean to the data. The**

834 **vertical grey dashed lines represent the minimum, median and maximum values of the 2000control**

835 **simulation across the 5 ensembles. Middle: monthly precipitation timeseries from the individual ensemble**

836 **members (thin curves) and the ensemble mean after applying a 10-year running mean (thick curves).**

837 **Right: precipitation trend from 2015 to 2100 for each month, with grey bars representing the climatology**

838 **from the 2000control experiment. In all panels, the noEP experiment is shown in blue and the EP**

839 **experiment is shown in orange.**

840

841

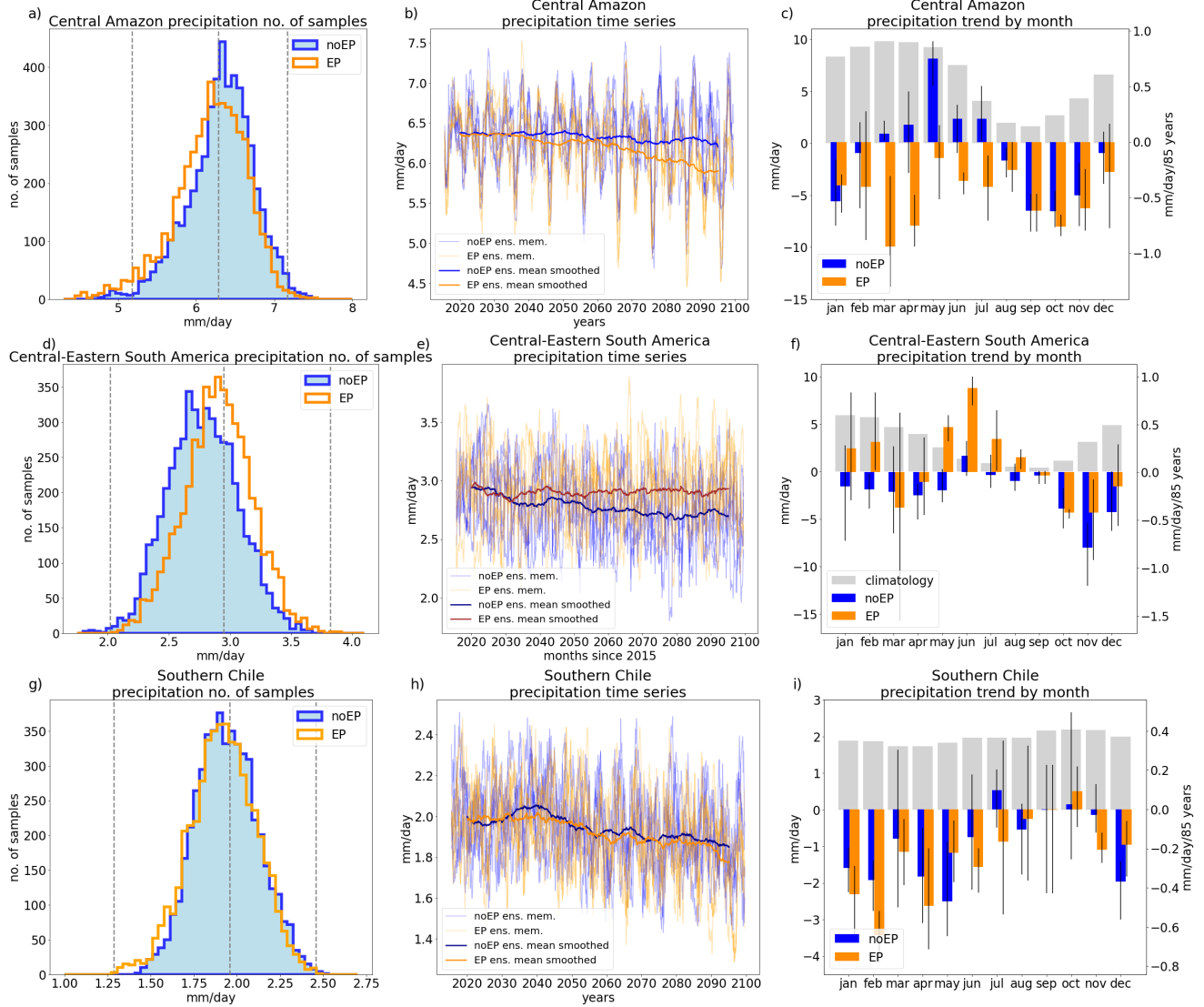
842

843

844

845

846



847

848

849

850

851

852

853

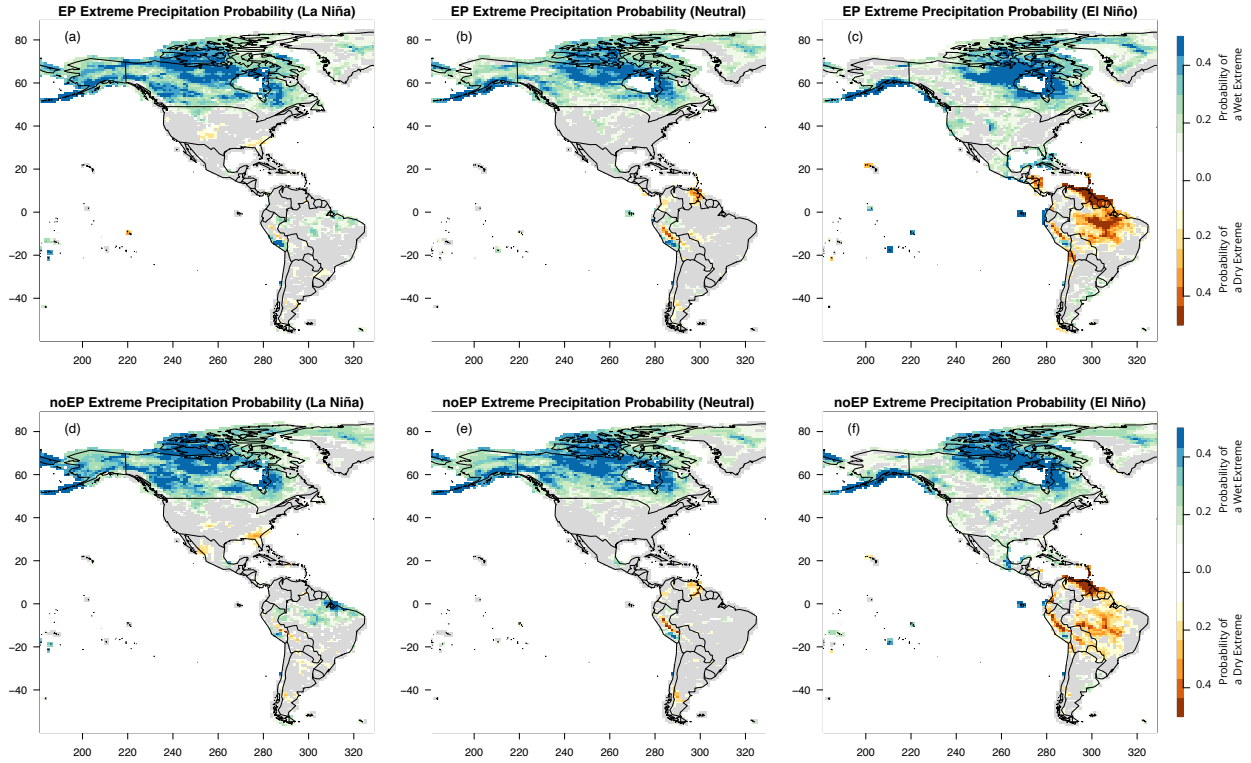
854

855

856

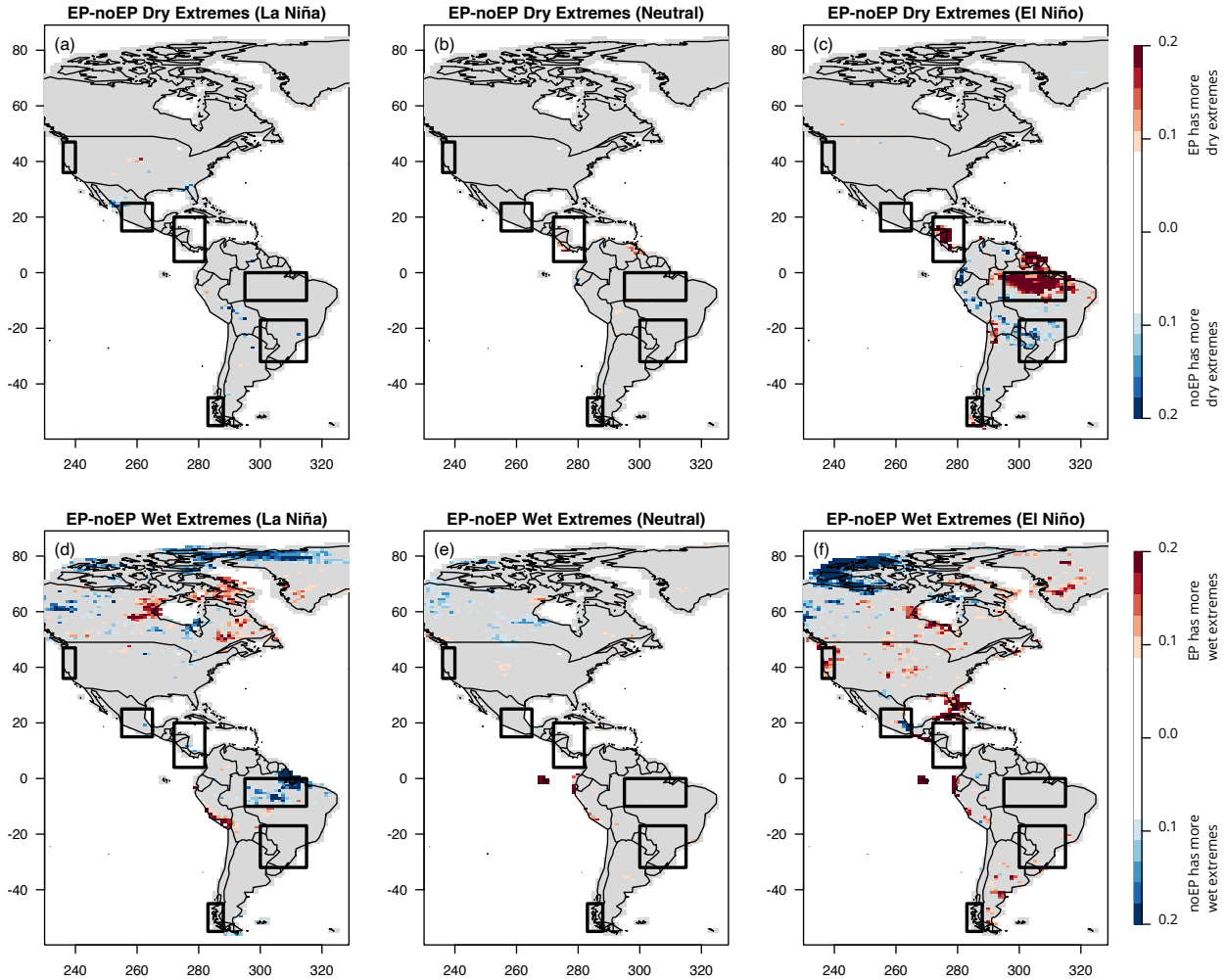
857

**Figure 6.** As in Fig. 5 but for the Central Amazon region, Central-Eastern South America and Southern Chile.



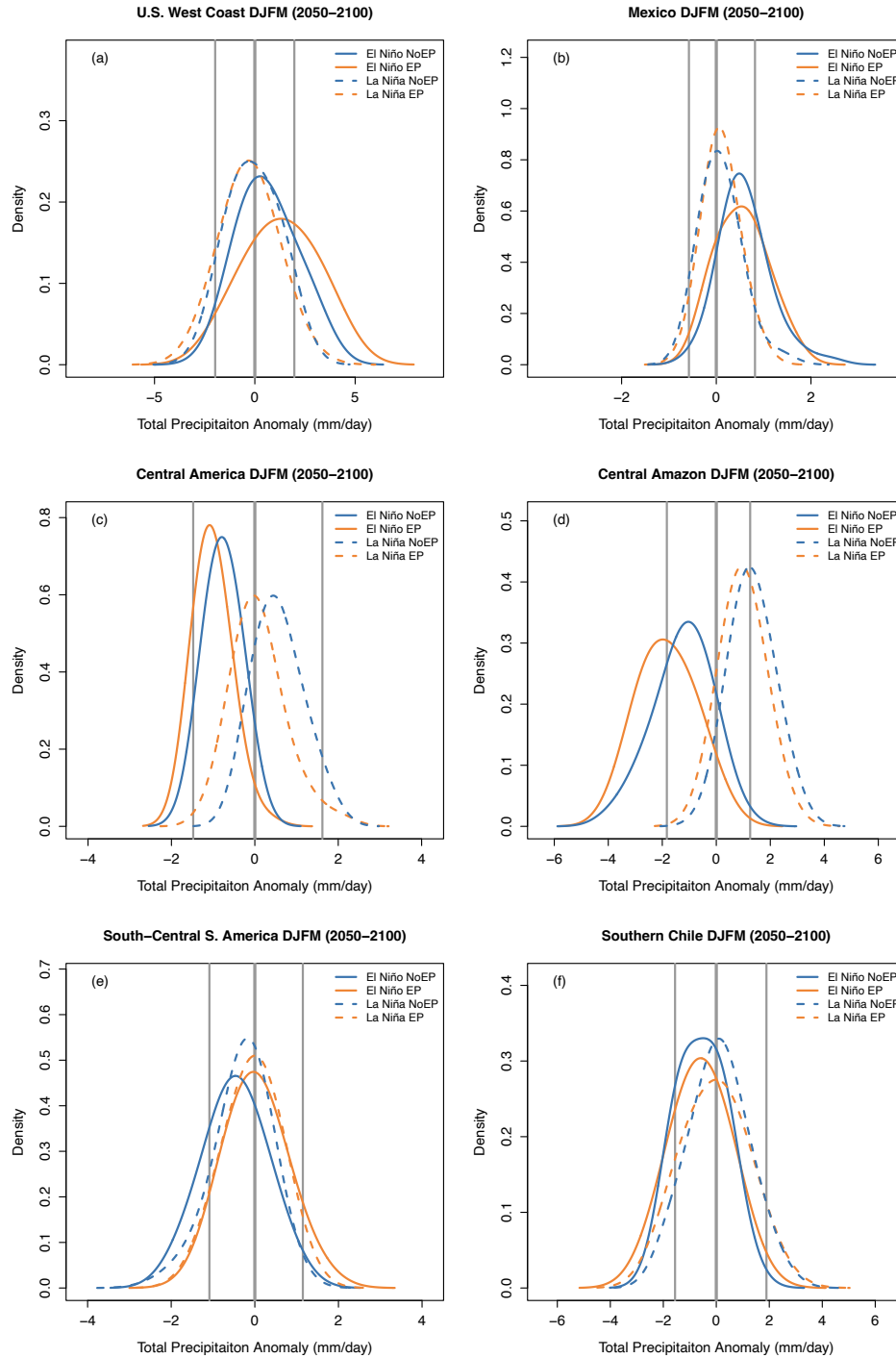
858  
859  
860  
861  
862  
863  
864  
865  
866  
867

**Figure 7. Frequency of 2050-2100 extreme DJFM precipitation in EP and noEP experiments during three phases of ENSO.** The empirical probability of extreme wet and dry DJFM in 2050-2100 during La Niña (left column), Neutral (middle column) and El Niño (right column) for the EP (first row) and the noEP (second row) experiments. Wet extremes are defined as a DJFM below the 2.5<sup>th</sup> percentile of the 2000control and dry extremes are defined as DJFM above the 97.5<sup>th</sup> percentile of the 2000control. Regions that do not have probabilities of wet or dry DJFM extremes statistically different from the 2000control are shaded in grey.



868  
869  
870  
871  
872  
873  
874  
875  
876  
877  
878  
879

**Figure 8.** The difference in the probability of dry and wet extreme DJFM between the EP and noEP experiments (2050-2100). The difference in the empirical probability of dry extremes (top row) and wet extremes (bottom row) as calculated as the difference of EP-noEP as shown in Figure 7. Red colors indicate an extreme DJFM is more likely under the EP experiment. The differences are shown for La Niña years (left column), for neutral years (middle column), and for El Niño years (right column). Areas that do not show a statistically significant difference in the rate of precipitation extremes between the EP and noEP experiments are shaded in grey.



880  
881  
882  
883  
884  
885  
886  
887

**Figure 9. Distribution of boreal winter precipitation anomalies during El Niño and La Niña in the EP and noEP experiments.** *Distribution of DJFM precipitation anomalies during 2050-2100 in the EP (orange) and noEP (blue) experiment relative to the Control experiment for El Niño (solid curves) and La Niña (dashed curves). The vertical grey lines indicate the mean, 2.5<sup>th</sup> and 97.5<sup>th</sup> percentiles of the Control experiment.*